New Journal of Physics
The open-access journal for physics

Mie scattering distinguishes the topological charge of an optical vortex: a homage to Gustav Mie

Valeria Garbin[1,5], Giovanni Volpe[2], Enrico Ferrari[3], Michel Versluis[1], Dan Cojoc[3] and Dmitri Petrov[2,4]

[1] Physics of Fluids Group—University of Twente, PO Box 217, 7500 AE Enschede, The Netherlands
[2] ICFO—Institut de Ciencies Fotoniques, Mediterranean Technology Park, Castelldefels, Barcelona 08860, Spain
[3] CNR-INFM, Laboratorio Nazionale TASC, Area Science Park—Basovizza, 30142 Trieste, Italy
[4] ICREA—Institucio Catalana de Recerca i Estudis Avancats, Passeig Llus Companys 23, Barcelona 08010, Spain

E-mail: v.garbin@utwente.nl, cojoc@tasc.infm.it and dmitri.petrov@icfo.es

New Journal of Physics **11** (2009) 013046 (11pp)
Received 5 June 2008
Published 26 January 2009
Online at http://www.njp.org/
doi:10.1088/1367-2630/11/1/013046

Abstract. One century after Mie's original paper, Mie scattering is still a fertile field of scientific endeavor. We show that the Mie scattering distinguishes the topological charge of light beams with phase dislocations. We experimentally and numerically study the scattering of highly focused Laguerre–Gaussian beams by dielectric and metal spheres, and show that the scattered field is sensitive to the modulus and to the sign of the topological charge. The implications for position detection systems are also discussed.

[5] Author to whom any correspondence should be addressed.

Contents

1. Introduction

Gustav Mie's theory, presented in his original 1908 paper [1] on the color of gold colloids, has found and continues to find wide application in various scientific disciplines including optical particle characterization, atmospheric science and astrophysics [2]–[5]. Mie considered the scattering of an infinite plane wave by a spherical particle. His approach has been subsequently extended to more general cases of practical interest, for instance to Gaussian and focused beams [6, 7] and to non-spherical particles [8].

Optical beams with a helical phase front such as Laguerre–Gaussian (LG) and Bessel beams attract significant interest in many areas of optics. The topological charge and associated orbital angular momentum of LG beams [9] gives rise to distinctive phenomena such as soliton generation [10], entanglement of photon quantum states [11], imaging [12] and orbital angular momentum exchange with atoms [13] and molecules [14]. The problem of the scattering of a laser beam exhibiting a helical phase front, thereby carrying a phase singularity, has received little attention up to now. Recently, the Mie scattering of LG beams by spherical particles was investigated theoretically in [15], for LG modes with different topological charges but the same handedness of the phase rotation.

LG beams have also found applications in optical trapping [16, 17]. Owing to their doughnut-like intensity distribution, LG beams are well suited to confine metal particles in two dimensions [18], to trap in three dimensions low-refractive index particles [19] and to increase the axial trapping efficiency for dielectric high-index particles [20]. A fundamental understanding of the interaction of LG beams with microparticles would therefore provide new possibilities for optical trapping applications. For instance, the question arises whether it is possible to use LG beams for back-focal plane interferometry, a technique for position detection of microparticles that is widely applied in photonic force microscopy [21]–[23].

It was also shown in optical trapping experiments that the orbital angular momentum associated with the helical phase of a LG beam can be transferred to a particle, inducing its rotation or gyration around the beam axis [24]–[27]. The optical torque that the beam exerts on the particle is clearly due to an asymmetric distribution of the total field at the sphere surface. As schematically illustrated in figure 1, a sphere displaced from the axis of a LG beam will experience an angular phase gradient, which has opposite sign depending on whether the topological charge is positive or negative. These observations implicitly indicate that, in addition to the observations of [15] the scattered field should be sensitive not only to the modulus but

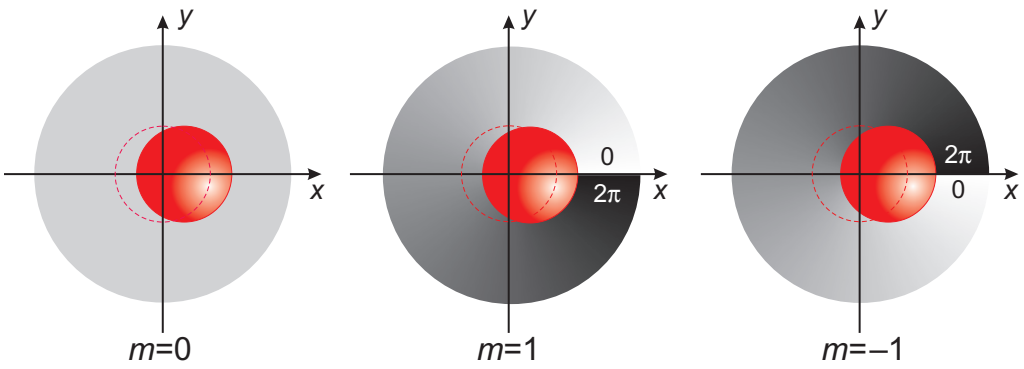

Figure 1. A sphere is displaced from the optical axis (z) along the x-direction for a Gaussian beam ($m = 0$) and for LG beams with $m = +1$ and -1. The phase fronts of the beams are shown in grayscale (from 0 to 2π the color changes from white to black). x is not a preferential direction in space with respect to the phase front of the LG beam, since the phase is periodic and its absolute value is arbitrary. For a Gaussian beam the phase front is plane and there is no phase gradient. A LG beam has an angular phase gradient which has different sign depending on the sign of the topological charge.

also to the *sign* of the phase rotation. Previous studies have shown agreement between theory and experiment for the case of optically trapped particles [28, 29].

Here, we show the effect of the spiral phase structure of a LG beam on the Mie scattering. In particular, we address the question whether the analysis of the scattered field (i.e. without observing the movement of an optically trapped particle due to the transfer of angular momentum) would enable us to distinguish the sign of the phase dislocation, as one would expect based on the arguments given above. We study the scattering from dielectric (non-absorbing) spheres and from metallic (strongly absorbing) spheres by varying both the modulus and the sign of the topological charge of the LG beam.

2. Theoretical approach

Our approach to the calculation of the scattering from an arbitrary focused beam on a spherical particle of arbitrary radius and refractive index is outlined in the following. We calculate the forward-scattered (FS) field and, by using an algorithm developed for position detection applications, we compute the response of a quadrant photodetector when the scattering sphere is moved off the optical axis. Details can be found in [30].

The incident beam is focused by an aplanatic lens producing a convergent spherical wave, which propagates to a diffraction-limited axial image. The aperture of the lens is taken as the entrance pupil of the optical system. A condenser lens collects the incident and FS fields. A position detector, located at a plane conjugated to the back-focal plane of the condenser lens, is used to quantify the variations in the total scattered field. The detector consists of four segments (A, B, C and D; see figure 2) with axes x and y. The intensities recorded on each segment are combined to give displacement signals corresponding to the directions x and y ($x = (\mathrm{A}+\mathrm{D}) - (\mathrm{B}+\mathrm{C})$ and $y = (\mathrm{A}+\mathrm{B}) - (\mathrm{C}+\mathrm{D})$).

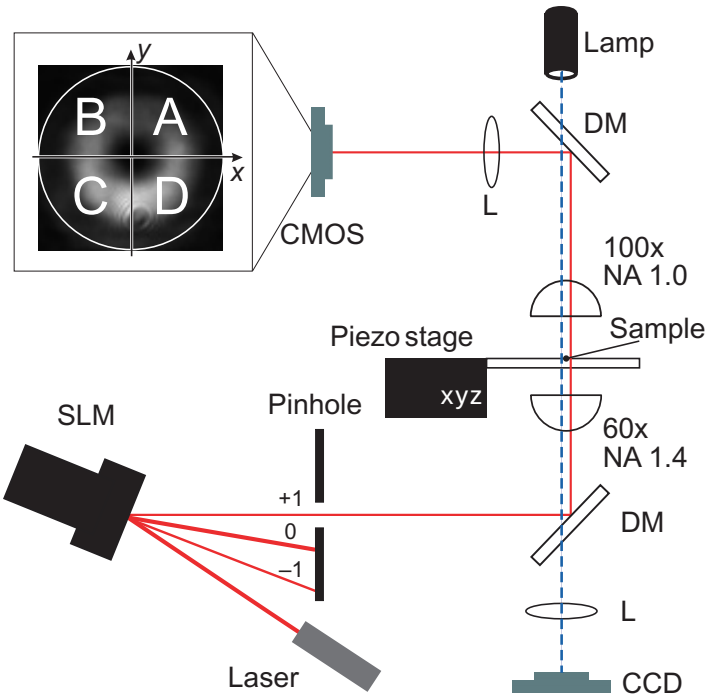

Figure 2. Experimental setup. SLM: spatial light modulator. DM: dichroic mirrors. CCD camera: for white light transmission imaging. CMOS camera: imaging of interference patterns. A diffractive optical element is implemented on the SLM for converting the Gaussian beam coming from the laser into a LG beam. The first diffraction order is selected with a pinhole and coupled into the 60× microscope objective. A 100× objective is used as a condenser to collect the light scattered by the sphere in the forward direction. The back-focal plane of the condenser is imaged onto the CMOS camera. The inset shows the segments configuration relative to the x and y axes of the translation stage. In experiments the spheres are always translated along x. The x- and y-signals correspond to changes in intensity in the x- and y-directions, respectively, and they are calculated from the intensities recorded at the four segments ($x = (\mathrm{A}+\mathrm{D}) - (\mathrm{B}+\mathrm{C})$, $y = (\mathrm{A}+\mathrm{B}) - (\mathrm{C}+\mathrm{D})$).

The main steps to compute the position detector response are:

1. calculate the distribution of the incident field near the focus of the lens;
2. solve the corresponding Mie–Debye problem, i.e. find the scattered wave for each partial plane wave describing the focused field for an arbitrary position of the sphere;
3. find the total scattered wave and propagate the total field at the back-focal plane of the condenser lens;
4. calculate the response of the position detector upon displacements of the sphere near the focal point.

For a LG beam, we write the incoming polarized wave $\mathbf{E}_i$ at the entrance plane of the focusing lens as

$$\mathbf{E}_i(\rho_i, \phi_i) = \mathbf{E}_i^{(0)} \mathrm{e}^{-\rho_i^2/w_0^2} (\rho_i/w_0)^{|m|} \mathrm{e}^{\mathrm{i}m\phi_i}, \tag{1}$$

where $\mathbf{E}_i^{(0)}$ describes the polarization of the incident field, assumed always linear, ρ_i and ϕ_i are the polar coordinates at the objective entrance and w_0 is the beam waist. The integer index m is the topological charge of the beam.

We verified our numerical algorithms by comparing the calculated response of the position detector with the results of [15] and found good agreement for the predicted behavior for metal particles. The numerical results corresponding to our experiments are presented in section 4.

3. Experimental setup

We investigated experimentally the Mie scattering of a focused LG beam by dielectric and metallic microspheres in a FS geometry. The experimental setup is shown schematically in figure 2. A LG beam was generated by converting the Gaussian beam coming from a fiber laser ($\lambda = 1064$ nm, linearly polarized) using diffractive optical elements (DOEs) implemented on a spatial light modulator (SLM) (Hamamatsu) [31]. The first diffraction order was selected using a pinhole and coupled by a dichroic mirror (DM) into a 60× objective (oil immersion, NA = 1.4, Nikon). The dynamic implementation of DOEs enabled us to switch between LG beams with different topological charge without changing the alignment of the beam and, in particular, keeping its focus always at the same position. This ensured that, for each sphere, we compare the FS with different beams under the same conditions. As the topological charge m of the beam is changed, the spiral structure is modified and as a consequence the radius of the annular high-intensity distribution changes. In particular, the radius of the high-intensity ring in the focal plane is proportional to the topological charge m [32]. In our experiments the modulus of the topological charge was varied between $|m| = 1$ and $|m| = 8$, and the radius of the high-intensity region increased from 0.9 to 3.1 μm. A 100× objective (water immersion, NA = 1.00, Olympus) was used as condenser lens to collect the FS light. The back-focal plane of the condenser was imaged by a lens (L) on a CMOS camera (Silicon Video). The sample plane was imaged on a CCD camera (DVC); the second DM transmitted white light for illumination of the sample, and directed the FS laser radiation on the CMOS camera. The video frames acquired with the CMOS camera were analyzed to quantify the variations in the FS field distribution upon particle displacement. To this aim, four detector segments were defined as described in section 2 (see also figure 2) and the corresponding x- and y-signals were computed from the video frames.

The aqueous suspension of microparticles was injected between two glass coverslips. We used the spheres that were adhering to the glass coverslip as probes. The sample was mounted on a xyz piezo translation stage (Piezosystem Jena) to scan the probes through the focused beam. In all the experiments, x is the direction of translation of the particle and y is the direction orthogonal to it. These are not preferential directions in space with respect to the phase front of the LG beam (see figure 1), since the phase is periodic and its absolute value is arbitrary. The results obtained by translating the sphere along x are therefore valid in general.

4. Results

4.1. Dielectric spheres

First, we investigated the effect of the modulus of the topological charge on dielectric particles. We used silica microspheres of radius $r_s = 0.5\,\mu$m (Bangs Laboratories). The particle size is comparable with the wavelength of light in the medium, and therefore with the waist w_0 of

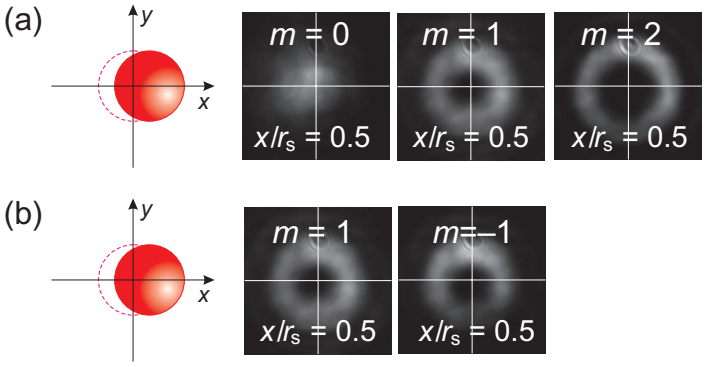

Figure 3. A dielectric sphere with radius $r_s = 0.5\,\mu$m is displaced off-axis in the x-direction. (a) Intensity distribution of the scattered field for $x/r_s = 0.5$, for a Gaussian beam ($m = 0$) and LG beams with $m = 1$ and 2. The effect of scanning the sphere through the beam is shown in movie 1 (442 kB, MOV): for a Gaussian beam the fringes move parallel to the direction of translation, x. For a LG beam the fringes move along a diagonal in the x–y plane. (b) Intensity distribution of the scattered field for $x/r_s = 0.5$ for LG beams with $m = +1$ and -1. When the sphere is scanned through the beam, the intensity pattern moves along opposite diagonals in the x, y plane, depending on the sign of the topological charge, as shown in movie 2 (326 kB, MOV). Both movies are available from stacks.iop.org/NJP/11/013046/mmedia.

the focused beam. The numerical simulations were performed on particles with a refractive index $n_{\text{silica}} = 1.5$ and using an effective NA for the lens to account for the partial filling of the objective's back-aperture (NA ~ 0.5).

The most remarkable effect observed in the Mie scattering of a LG beam with topological charge $m \neq 0$ is that for a displacement of the scatterer along the x-direction, the total scattered field changes also in the y-direction. The simulations also revealed this property of the scattered field, which was already predicted in [15] for metal spheres.

Figure 3(a) shows the intensity patterns recorded on the CMOS camera upon displacement of a sphere along the x-direction ($x/r_s = 0.5$) for different values of the topological change, $m = 0$, 1 and 2. When the sphere is off-axis, for a Gaussian beam ($m = 0$) the interference fringes in the back-focal plane move off-center, parallel to the direction of translation of the particle. For a LG beam with $m = 1$ or 2, the high-intensity region of the interference pattern moves at an angle with the direction of displacement. The corresponding movie (movie 1, available from stacks.iop.org/NJP/11/013046/mmedia) illustrates this effect: the high-intensity part of the interference fringes for $m = 1$ and 2 is moving along a diagonal in the x, y plane. This effect is due to the phase front of the LG beam, as schematically represented in figure 1: the phase of a Gaussian beam (topological charge $m = 0$) is mirror symmetric with respect to any direction orthogonal to the optical axis (e.g. x), but this is not the case for a LG beam ($m \neq 0$).

To investigate the effect of the handedness of the helical phase front, we then inverted the sign of the topological charge of the incident beam. Figure 3(b) shows that the high-intensity region of the interference pattern moves along two opposite diagonals in the x, y plane for $m = 1$ and -1, an effect which is also clearly visible in movie 2.

To quantify the changes in the spatial distribution of the scattered field we calculated from the video frames the position signals as outlined in section 3. Figure 4 compares the

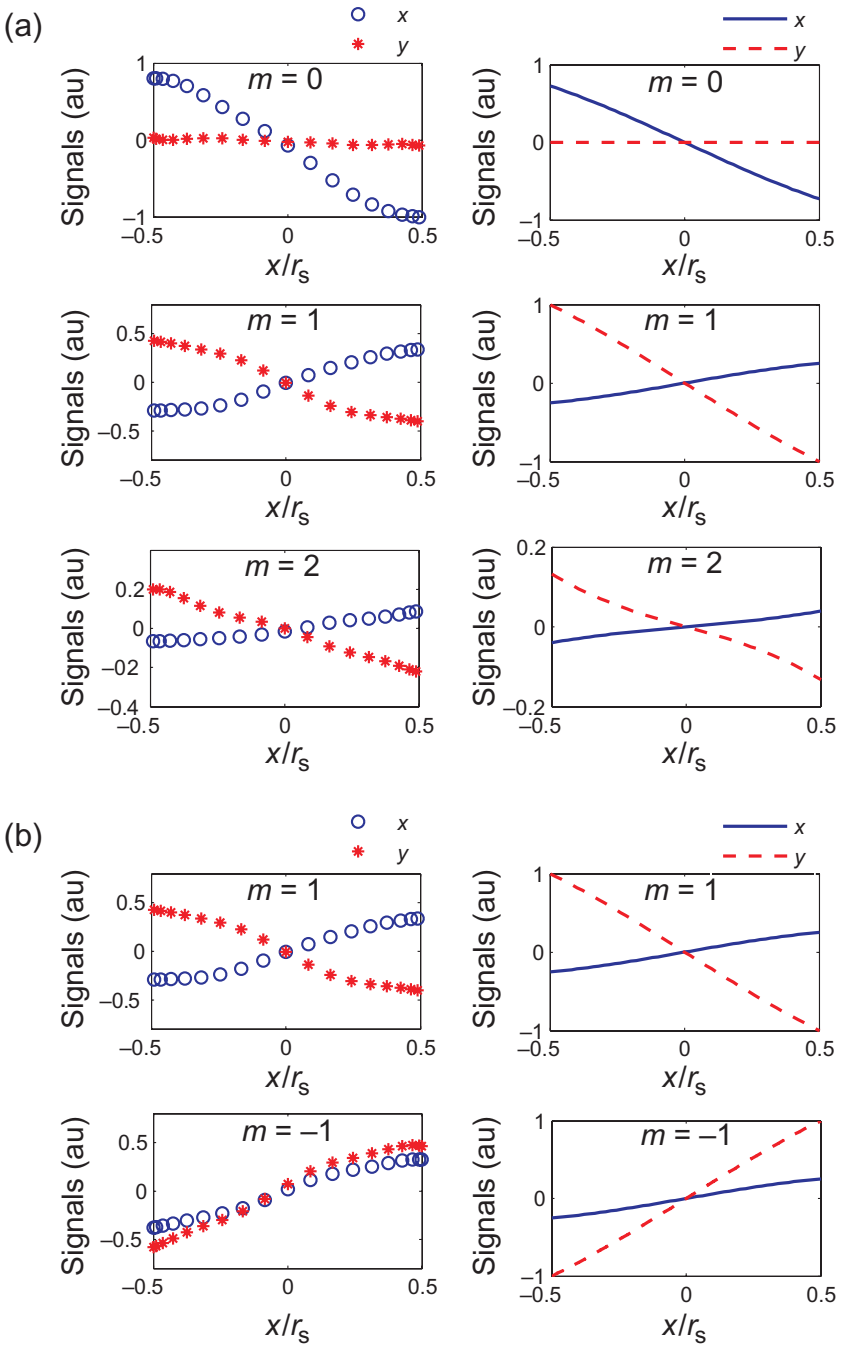

Figure 4. x- and y-signals for a dielectric sphere ($r_s = 0.5\,\mu$m) as the particle is translated along x. The left column shows the experimental results (x: circles and y: stars) obtained for beams with different modulus of the topological charge (a) and for LG beams with different sign of the charge (b). The right column presents the corresponding simulations (x: solid line and y: dashed line). For a Gaussian beam the y-response is zero (no cross-talk); for a LG beam ($m = 1, 2$), the y-response can also be measured, as predicted by the simulations. For opposite values of the topological charge ($m = 1$ and -1) the x-response is unchanged, whereas the y-response changes sign.

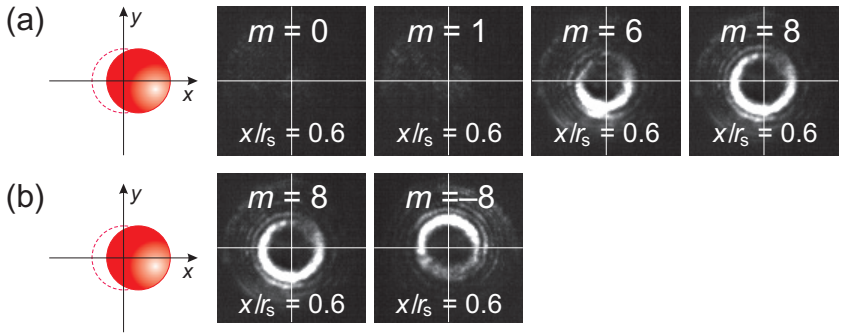

Figure 5. A metal sphere with radius $r_s = 3.5\,\mu$m is displaced from the center of the beam in the x-direction. (a) Intensity distribution of the scattered beam when the sphere is positioned at $x/r_s = 0.5$ for a Gaussian beam ($m = 0$) and LG beams with $m = 1$, 6 and 8. For $m = 0$ and for small values of m, the doughnut radius is much smaller than the radius of the sphere, so that the incident beam is completely blocked and almost no intensity is detected for small displacements ($-0.5 < x/r_s < 0.5$). For $m \geqslant 6$ the doughnut radius becomes comparable with the particle radius. An interference pattern is recorded, with a strong displacement in the y-direction. This effect is shown in movie 3, where the particle is scanned through the beam (372 kB, MOV). (b) Effect of the sign of the topological charge: the y-component of the intensity pattern moves in opposite directions for $m = 8$ and -8. The effect of scanning the sphere through the beam is illustrated in movie 4 (238 kB, MOV). Both movies are available from stacks.iop.org/NJP/11/013046/mmedia.

experimental x- and y-signals (left column) with the ones obtained by the numerical simulations (right column). The main features observed in the experiments are captured by the simulations. In particular, figure 4(a) shows that for a Gaussian beam ($m = 0$) the y-signal is negligible and only an x-response is observed. For a LG beam with $m = 1$ or 2, a strong y-response is also measured, corresponding to the diagonal displacement of the intensity pattern showed in figure 3(a). We also note that for $m = 1$ the slope of the x-signal near $x/r_s = 0$ has opposite sign than that for $m = 0$, and the sign of the slope is conserved for $m = 2$. The change in the slope of the x-response can be ascribed to the change in size of the doughnut with increasing topological charge: for $m = 0$ the radius of the Gaussian spot is comparable with the sphere radius; $m = 1$ corresponds to the cross-over to a range where the beam radius is larger than the sphere radius.

The effect of changing the sign of m is shown in figure 4(b). For $m = 1$ and -1 the x-response is unchanged, whereas the slope of the y-response near $x/r_s = 0$ changes sign.

4.2. Absorbing spheres

We also studied how the modulus and sign of the topological charge of the incident beam affect the scattered field for the case of absorbing particles. We used gold-coated polystyrene spheres with radius $r_s = 3.5\,\mu$m (Microparticles GmbH). The numerical simulations were performed assuming a refractive index $n_{\text{gold}} = 0.503 + i4.923$ and NA ~ 0.5.

Figure 5(a) shows the intensity patterns recorded on the CMOS camera upon displacement of the sphere along the x-direction for $m = 0$ (Gaussian beam), 1, 6 and 8. For $m = 0$

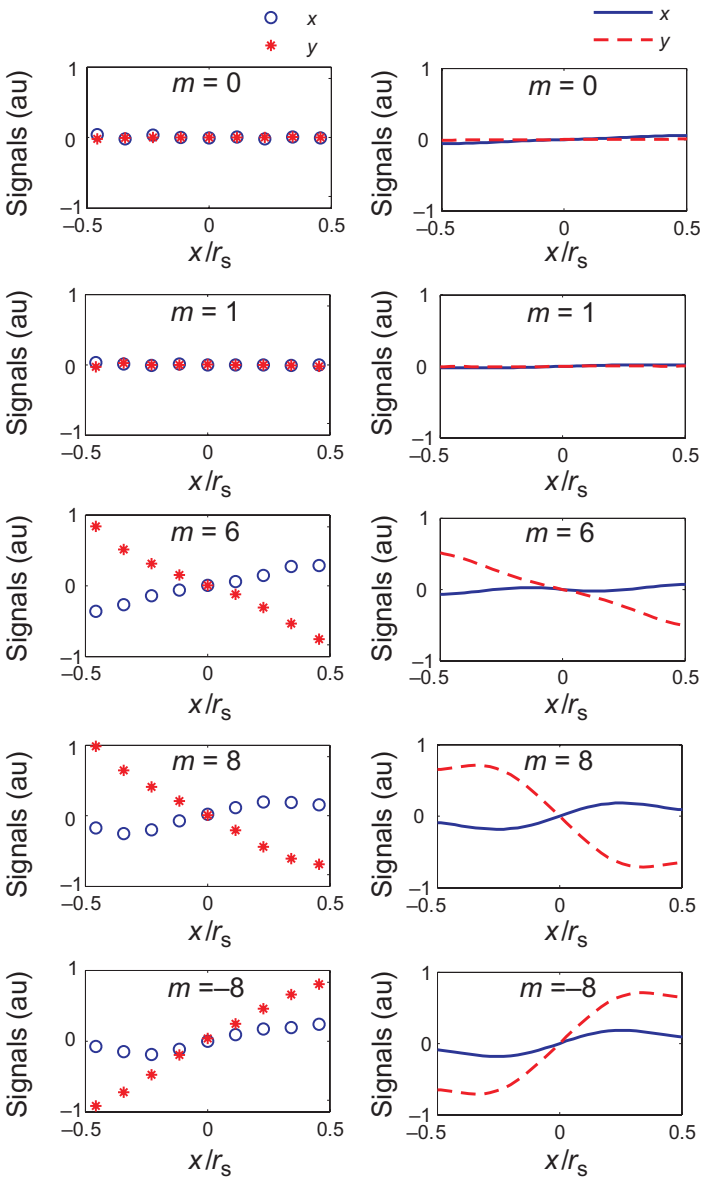

Figure 6. x- and y-signals for a metal sphere with radius $r_s = 3.5\,\mu$m scanned along the x-direction. The left column shows the experimental results (x: circles and y: stars) and the right column presents the corresponding simulations (x: solid line and y: dashed line). For $m = 0$ and 1 both position signals are negligible, because the particle blocks the incident beam. For larger doughnut size ($m = 6$ and 8) a x-response is measured for a displacement along x, but most remarkably an even bigger y-component is observed. When the sign of m is reversed, the y-response changes sign as predicted by the simulations.

($w_0 = 0.7\,\mu$m) and for LG beams with small values of m, the radius of the doughnut is much smaller than the sphere radius. Hence, the incident beam is completely reflected when the sphere is on-axis, and almost no scattered intensity is detected in the forward direction. Even for small displacements of the sphere ($-0.5 < x/r_s < 0.5$) the incident beam remains blocked. For a LG beam with $m \geqslant 6$ the doughnut radius becomes comparable with the particle radius,

and an interference pattern can now be recorded at the detector plane. Large displacements of the intensity pattern in the y-direction are observed when the sphere is translated off-axis ($x/r_s = 0.6$), as illustrated in movie 3 (available from stacks.iop.org/NJP/11/013046/mmedia), where the sphere is scanned through the beam. In figure 5(b), the effect of the sign of the topological charge is shown: the intensity pattern moves in opposite directions along y for LG beams with $m = 8$ and -8 as illustrated in movie 4.

Figure 6 compares the position signal obtained in the experiments (left column) with those from the simulations (right column). For a Gaussian beam and for LG beams with topological charge up to $m = 5$ (only $m = 0$ and 1 are shown in the figure) a low scattered intensity is detected, and only for large off-axis displacements of the particle ($x/r_s > 0.5$), i.e. when a part of the incident beam is unblocked. For LG beams with $m \geqslant 6$ the slope of the responses around $x/r_s = 0$ becomes nonzero (for $m = 6$ the radius of the doughnut is $r_{I_{max}} = 2.7\,\mu$m). Also in the case of metal spheres a strong y-response is measured which, notably, is larger than the x-response. Like for the case of dielectric spheres, a change in the sign of the topological charge leaves the slope of the x-response unchanged, while the y-response changes sign (see $m = 8$ and -8 in the figure).

5. Conclusions

The scattering of a LG beam by a sphere generates a field that is sensitive both to the modulus and the sign of the topological charge of the incident beam. This sensitivity manifests itself when the sphere is displaced off the beam axis, and it can be studied qualitatively by measuring the spatial distribution of the scattered field. We investigated this effect for dielectric and metal spheres in focused LG beams through experiments and numerical simulations.

Our experiments indicate that, in the case of dielectric particles, there is a significant cross-talk between the position signals obtained with a quadrant detector configuration. However, there is a range where the signals change linearly with the sphere displacement. The method for inferring the position of a particle from the quadrant detector signals is beyond the scope of the present work, and will be addressed elsewhere. These observations show the potential for position detection of dielectric particles using LG beams.

Acknowledgments

GV thanks Gregory Kozyreff for many useful discussions. VG is supported by a Rubicon grant of the Netherlands Organization for Scientific Research (NWO) and by the Interuniversity Cardiology Institute of the Netherlands (ICIN). This research was supported in part by the Spanish Ministry of Education and Science (Grant No. NAN2004-09348-C04-02), by the Departament d'Universitats, Recerca i Societat de la Informació, and by the European Social Fund.

References

[1] Mie G 1908 Beiträge zur Optik trüber Medien, speziell kolloidaler Metallösungen *Ann. Phys., Lpz.* **25** 377–445
[2] Born M and Wolf E 1999 *Principles of Optics* 7th edn (Cambridge: Cambridge University Press)
[3] Kerker M 1969 *The Scattering of Light and Other Electromagnetic Radiation* (New York: Academic)
[4] van de Hulst H C 1981 *Light Scattering by Small Particles* (New York: Dover)

[5] Goody R M and Yung Y L 1989 *Atmospheric Radiation: Theoretical Basis* (New York: Oxford University Press)
[6] Gouesbet G, Grehan G and Maheu B 1985 Scattering of a Gaussian beam by a Mie scatter center using a Bromwich formalism *J. Opt.* **16** 83–93
[7] Barton J P, Alexander D R and Schaub S A 1988 Internal and near-surface electromagnetic fields for a spherical particle irradiated by a focused laser beam *J. Appl. Phys.* **64** 1632–9
[8] Han Y P, Grehan G and Gouesbet G 2003 Generalized Lorenz–Mie theory for a spheroidal particle with off-axis Gaussian-beam illumination *Appl. Opt.* **42** 6621–9
[9] Allen L, Barnett S M and Padgett M 2003 *Optical Angular Momentum* (Bristol: Institute of Physics Publishing)
[10] Desyatnikov A S, Torner L and Kivshar Y S 2005 *Optical Vortices and Vortex Solitons Progress in Optics* vol 47 ed E Wolf (Oxford: Pergamon)
[11] Mair A, Vaziri A, Weihs G and Zeilinger A 1990 Entanglement of the orbital angular momentum states of photons *Nature* **412** 313–6
[12] Torner L, Torres J P and Carrasco S 2005 Digital spiral imaging *Opt. Express* **13** 873–81
[13] Jáuregui R 2004 Rotational effects of twisted light on atoms beyond the paraxial approximation *Phys. Rev.* A **70** 033415
[14] Alexandrescu A, Cojoc D and Di Fabrizio E 2006 Mechanism of angular momentum exchange between molecules and Laguerre–Gaussian beams *Phys. Rev. Lett.* **96** 243001
[15] van de Nes A S and Török P 2007 Rigorous analysis of spheres in Gauss–Laguerre beam *Opt. Express* **15** 13360–74
[16] Molloy J E and Padgett M 2002 Lights, action: optical tweezers *Contemp. Phys.* **43** 241–58
[17] Grier D G 2003 A revolution in optical manipulation *Nature* **424** 810–6
[18] Sato S, Harada Y and Waseda Y 1994 Optical trapping of microscopic metal particles *Opt. Lett.* **19** 1807–9
[19] Gahagan K T and Swartzlander G A 1996 Optical vortex trapping of particles *Opt. Lett.* **21** 827–9
[20] O'Neil A T and Padgett M J 2001 Axial and lateral trapping efficiency of Laguerre–Gaussian modes in inverted optical tweezers *Opt. Commun.* **193** 45–50
[21] Ghislain L P and Webb W W 1993 Scanning-force microscope based on an optical trap *Opt. Lett.* **18** 1678–80
[22] Prälle A, Prummer M, Florin E-L, Stelzer E H K and Hörber J K H 1999 Three-Dimensional high-resolution particle tracking for optical tweezers by forward scattered light *Microsc. Res. Tech.* **44** 378–86
[23] Volpe G, Volpe G and Petrov D 2007 Brownian motion in a nonhomogeneous force field and photonic force microscope *Phys. Rev.* E **76** 061118
[24] He H, Friese M E J, Heckenberg N R and Rubinsztein-Dunlop H 1995 Direct observation of transfer of angular momentum to absorptive particles from a laser beam with a phase singularity *Phys. Rev. Lett.* **75** 826–9
[25] Paterson L, MacDonald M P, Arlt J, Sibbett W, Bryant P E and Dholakia K 2001 Controlled rotation of optically trapped microscopic particles *Science* **292** 912–4
[26] O'Neil A T, MacVicar I, Allen L and Padgett M J 2002 Intrinsic and extrinsic nature of the orbital angular momentum of a light beam *Phys. Rev. Lett.* **88** 053601
[27] Volpe G and Petrov D 2006 Torque Detection using Brownian Fluctuations *Phys. Rev. Lett.* **97** 210603
[28] Simpson N B, Dholakia K, Allen L and Padgett M J 1997 Mechanical equivalence of spin and orbital angular momentum of light: an optical spanner *Opt. Lett.* **22** 52–4
[29] Zhao Y, Edgar J S, Jeffries G D M, McGloin D and Chiu D T 2007 Spin-to-orbital angular momentum conversion in a strongly focused optical beam *Phys. Rev. Lett.* **99** 073901
[30] Volpe G, Kozyreff G and Petrov D 2007 Backscattering position detection for photonic force microscopy *J. Appl. Phys.* **102** 084701
[31] Cojoc D, Garbin V, Ferrari E, Businaro L, Romanato F and Di Fabrizio E 2005 Laser trapping and micro-manipulation using Laguerre–Gaussian beams *Microelectron. Eng.* **78–79** 125–31
[32] Curtis J E and Grier D G 2003 Structure of optical vortices *Phys. Rev. Lett.* **90** 133901